NANO LETTERS

Letter

Cite This: Nano Lett. 2019, 19, 2371−2376

pubs.acs.org/NanoLett

New Generation of Moiré Superlattices in Doubly Aligned hBN/Graphene/hBN Heterostructures

Lujun Wang,*[,†,⊥] Simon Zihlmann,[†] Ming-Hao Liu,[‡] Péter Makk,[†,§] Kenji Watanabe,[∥] Takashi Taniguchi,[∥] Andreas Baumgartner,*[,†,⊥] and Christian Schönenberger[†,⊥]

[†]Department of Physics, University of Basel, Klingelbergstrasse 82, CH-4056 Basel, Switzerland

[⊥]Swiss Nanoscience Institute, University of Basel, Klingelbergstrasse 82, CH-4056 Basel, Switzerland

[‡]Department of Physics, National Cheng Kung University, Tainan 70101, Taiwan

[§]Department of Physics, Budapest University of Technology and Economics and Nanoelectronics Momentum Research Group of the Hungarian Academy of Sciences, Budafoki ut 8, 1111 Budapest, Hungary

[∥]National Institute for Material Science, 1-1 Namiki, Tsukuba, 305-0044, Japan

Supporting Information

ABSTRACT: The specific rotational alignment of two-dimensional lattices results in a moiré superlattice with a larger period than the original lattices and allows one to engineer the electronic band structure of such materials. So far, transport signatures of such superlattices have been reported for graphene/hBN and graphene/graphene systems. Here we report moiré superlattices in fully hBN encapsulated graphene with both the top and the bottom hBN aligned to the graphene. In the graphene, two different moiré superlattices form with the top and the bottom hBN, respectively. The overlay of the two superlattices can result in a third superlattice with a period larger than the maximum period (14 nm) in the graphene/hBN system, which we explain in a simple model. This new type of band structure engineering allows one to artificially create an even wider spectrum of electronic properties in two-dimensional materials.

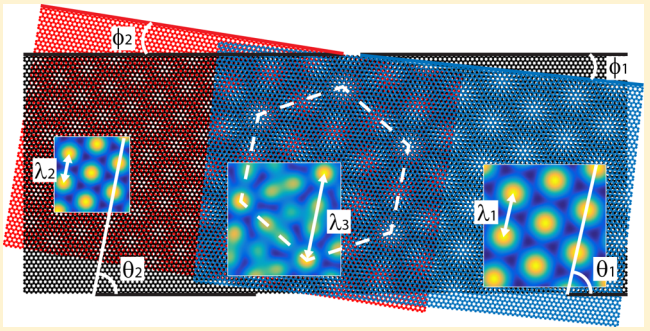

KEYWORDS: *hBN encapsulated graphene, moiré superlattice, three-layer moiré pattern, superlattice Dirac point, twistronics*

Superlattice (SL) structures have been used to engineer electronic properties of two-dimensional electron systems for decades.[1−8] Because of the peculiar electronic properties of graphene,[9] SLs in graphene are of particular interest[10−16] and have been investigated extensively utilizing different approaches, such as electrostatic gating,[17−19] chemical doping,[20] etching,[21−23] lattice deformation,[24] and surface dielectric patterning.[25] Since the introduction of hexagonal boron nitride (hBN) as a substrate for graphene electronics,[26] moiré superlattices (MSLs) originating from the rotational alignment of the two lattices have been first observed and studied by scanning tunneling microscopy (STM).[27−29] It then triggered many theoretical[30−33] and experimental studies, where secondary Dirac points,[34−36] the Hofstadter Butterfly,[34−38] Brown-Zak oscillations,[34−39] the formation of valley polarized currents,[40] and many other novel electronic device characteristics[41−46] have been observed.

Recently, another interesting graphene MSL system has drawn considerable attention, the twisted bilayer graphene, where two monolayer graphene sheets are stacked on top of each other with a controlled twist angle. For small twist angles, insulating states,[47] strong correlations,[48] and a network of topological channels[49] have been reported experimentally. More strikingly, superconductivity[50,51] and Mott-like insulator states[51,52] have been achieved, when the twist angle is tuned to the so-called "magic angle", where the electronic band structure near zero Fermi energy becomes flat, due to the strong interlayer coupling.

So far, MSL engineering in graphene has concentrated mostly on MSLs based on two relevant layers (2L-MSLs). However, fully encapsulated graphene necessarily forms two interfaces, namely at the top and at the bottom, which can result in a much richer and more flexible tailoring of the graphene band structure. Because of the 1.8% larger lattice constant of hBN, the largest possible moiré period that can be achieved in graphene/hBN systems is limited to about 14 nm,[29] which occurs when the two layers are fully aligned. This situation changes when both hBN layers are aligned to the graphene layer. Here, we report the observation of a new MSL which can be understood by the overlay of two 2L-MSLs that form between the graphene monolayer and the top and bottom hBN layers of the encapsulation stack, respectively. Figure 1

Received: December 19, 2018
Revised: February 21, 2019
Published: February 25, 2019

DOI: 10.1021/acs.nanolett.8b05061
Nano Lett. 2019, 19, 2371−2376

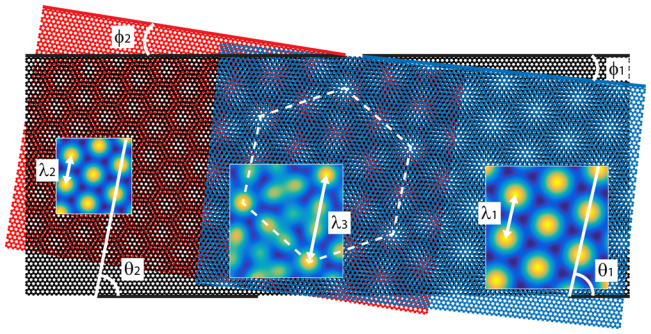

Figure 1. Illustration of three different MSLs formed in a hBN/graphene/hBN heterostructure. Blue, black, and red hexagonal lattices represent top hBN, graphene, and bottom hBN lattices, respectively. ϕ_1 (ϕ_2) is the twist angle between top (bottom) hBN and graphene. θ_1 (θ_2) indicates the orientation of the corresponding MSL with respect to graphene. The resulting moiré periods are indicated with $\lambda_{1,2,3}$. The 3L-MSL (middle part) has a larger period than both 2L-MSLs (left and right parts). Insets: moiré potential calculations.

illustrates the formation of the MSLs when both hBN layers are considered. On the right side of the illustration, only the top hBN (blue) and the graphene (black) are present, which form the top 2L-MSL with period λ_1. The bottom hBN (red) forms the bottom 2L-MSL with graphene, shown on the left with period λ_2. In the middle of the illustration, all three layers are present and a new MSL (3L-MSL) forms with a longer period, indicated with λ_3. The influence of the MSL can be modeled as an effective periodic potential with the same symmetry. The periodic potentials for the top 2L-MSL and the bottom 2L-MSL are calculated following the model introduced in ref 29, shown as insets in Figure 1. To calculate the potentials for the 3L-MSL, we sum over the periodic potentials of the top 2L-MSL and the bottom 2L-MSL. The period of the 3L-MSL from the potential calculation matches very well the one of the lattice structure in the illustration. In the transport measurements, we demonstrate that MSL with a period longer than 14 nm can indeed be obtained in doubly aligned hBN/graphene/hBN heterostructures, coexisting with the graphene/hBN 2L-MSLs. These experiments are in good agreement with a simple model for the moiré periods for doubly aligned hBN/graphene/hBN devices.

We fabricated fully encapsulated graphene devices with both the top and the bottom hBN layers aligned to the graphene using a dry-transfer method.[53] We estimate an alignment precision of ~1°. A global metallic bottom gate is used to tune the charge carrier density n, and one-dimensional Cr/Au edge contacts are used to contact the graphene[53] (see inset of Figure 2a). Transport measurements were performed at 4.2 K using standard low-frequency lock-in techniques.

The two-terminal differential conductance, G, of one device, shown as inset of Figure 2c, is plotted as a function of n in Figure 2a (data from other devices with similar characteristics, including bilayer graphene devices, are presented in the Supporting Information). The charge carrier density n is calculated from the gate voltage using a parallel plate capacitor model. The average conductance is lower on the hole side ($n < 0$) than on the electron side ($n > 0$), which we attribute to n-type contact doping resulting in a p−n junction near the contacts. The sharp dip in conductance at $n = 0$ is the main Dirac point (MDP) of the pristine graphene. Our device shows a large field-effect mobility of ~90 000 cm^2 V^{-1} s^{-1}, extracted from a linear fit around the MDP. The residual doping is of the

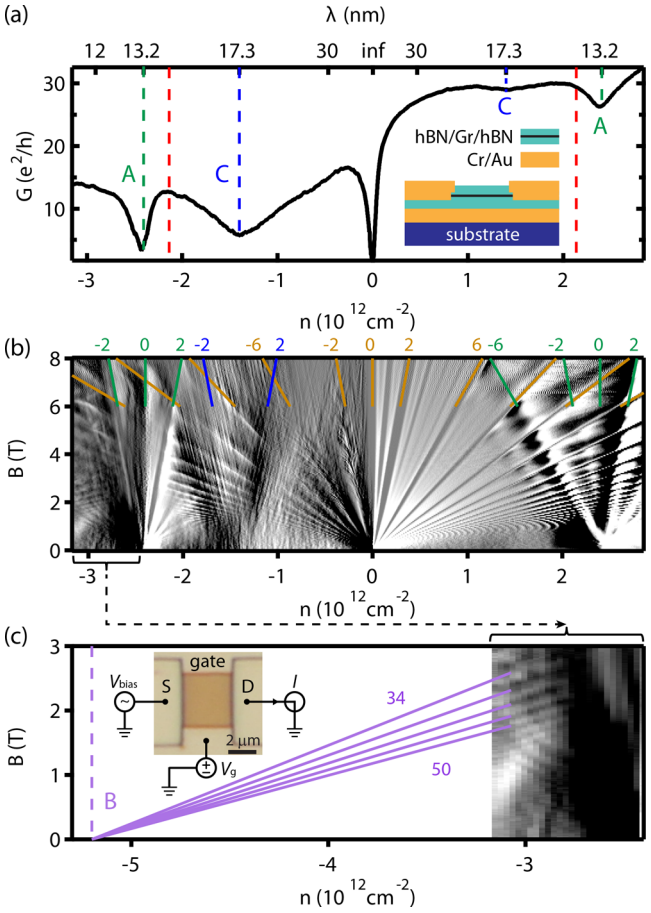

Figure 2. Electronic transport at 4.2 K. (a) Two-terminal differential conductance G as a function of charge carrier density n. In addition to the MDP, there are four other conductance minima at $n_{s_A} \approx \pm 2.4 \times 10^{12}$ cm^{-2} (green dashed lines) and $n_{s_C} \approx \pm 1.4 \times 10^{12}$ cm^{-2} (blue dashed lines), respectively. The top axis shows the moiré periods $\lambda = \sqrt{4\pi/3n_s}$. The red dashed lines indicate the longest period (lowest density) for a graphene/hBN MSL. Inset: schematic of the cross section of our device. (b) dG/dn as a function of n and B of the same device. Filling factors fan out from all DPs, except for the blue one on the electron side and are indicated on top of the diagram, calculated as $\nu \equiv nh/(eB)$, where n is counted from each DP. (c) Zoom-in on the left side of (b). There are additional lines fanning out from an even higher density $n_{s_B} \approx 5.2 \times 10^{12}$ cm^{-2}, labeled B. The filling factors of these lines are 34, 38, 42, 46 and 50, respectively. Inset: micrograph and experimental setup of the presented device. "S" and "D" are the source and drain contacts, respectively.

order $\delta n \approx 1 \times 10^{10}$ cm^{-2}, extracted from the width of the MDP. In addition to the MDP, we find two pairs of conductance minima symmetrically around the MDP at higher doping, labeled A and C, which we attribute to two MSLs. The minima on the hole side are more pronounced than their counterparts on the electron side, similar to previously reported MSLs.[29,34−36]

On the basis of the simple model of periodic potential modulation,[11,29,31] superlattice Dirac points (SDPs) are expected to form at the superlattice Brillouin zone boundaries at $\mathbf{k} = \mathbf{G}/2$, where $|\mathbf{G}| = 4\pi/(\sqrt{3}\lambda)$ is the length of the superlattice wavevector and λ is the moiré period. For graphene, k is related to n by $k = \sqrt{\pi n}$. The position of the SDPs in charge carrier density for a given period λ is then $n_s =$

DOI: 10.1021/acs.nanolett.8b05061
Nano Lett. 2019, 19, 2371−2376

$4\pi/(3\lambda^2)$. The pair of conductance minima at $n_{s_A} \approx \pm 2.4 \times 10^{12}$ cm^{-2} can be explained by a graphene/hBN 2L-MSL with a period of about 13.2 nm. However, the pair of conductance minima at $n_{s_C} \approx \pm 1.4 \times 10^{12}$ cm^{-2} cannot be explained by a single graphene/hBN 2L-MSL, because it corresponds to a superlattice period of about 17.3 nm, clearly larger than the maximum period of ~14 nm in a graphene/hBN moiré system. We attribute the presence of the conductance dips at n_{s_C} to a new MSL that is formed by the three layers together: top hBN, graphene and bottom hBN. This 3L-MSL can have a period considerably larger than 14 nm.

To substantiate this claim, we now analyze the data obtained in the quantum Hall regime. Figure 2b shows the Landau fan of the same device, where the numerical derivative of the conductance with respect to n is plotted as a function of n and the out-of-plane magnetic field B. Near the MDP, we observe the standard quantum Hall effect for graphene with plateaus at filling factors $\nu \equiv nh/(eB) = \pm 2, \pm 6, \pm 10, \ldots$ with h as the Planck constant and e as the electron charge. This spectrum shows the basic Dirac nature of the charge carriers in graphene. The broken symmetry states occur for $B \geqslant 2$T, suggesting a high device quality. Around the SDPs at $n_{s_A} \approx \pm 2.4 \times 10^{12}$cm^{-2}, the plot also shows filling factors $\nu \equiv (n - n_{s_A})h/(eB) = \pm 2, \pm 6, \ldots$ consistent with previous graphene/hBN MSL studies.[34] Around the SDPs at $n_{s_C} \approx \pm 1.4 \times 10^{12}$ cm^{-2}, there are also clear filling factors fanning out on the hole side with $\nu \equiv (n - n_{s_C})h/(eB) = \pm 2$, which is consistent with a Dirac spectrum at n_{s_C}, while on the electron side the corresponding features are too weak to be observed. In addition, lines fanning out from a SDP located at density $n < -3 \times 10^{12}$ cm^{-2} are observed. A zoom-in is plotted in Figure 2c. The lines extrapolate to a density of about -5.2×10^{12} cm^{-2}, denoted n_{s_B} with filling factors $\nu = 34, 38, 42, 46, \ldots$ This density cannot be explained by the "tertiary" Dirac point occuring at the density of about $1.65n_{s_A}$, which comes from a Kekulé superstructure on top of the graphene/hBN MSL.[54] However, n_{s_B} matches the SDP from a MSL with a period of about 9 nm. We therefore attribute it to a 2L-MSL originating from the alignment of the second hBN layer to the graphene layer.

As derived in refs 29 and 33, the period λ for a graphene/hBN MSL is given by

$$\lambda = \frac{(1+\delta)a}{\sqrt{2(1+\delta)(1-\cos\phi)+\delta^2}} \quad (1)$$

where a (2.46 Å) is the graphene lattice constant, δ (1.8%) is the lattice mismatch between hBN and graphene and ϕ (defined for −30° to 30°) is the twist angle of hBN with respect to graphene. The moiré period is maximum at $\phi = 0$ with a value of $\lambda \approx 14$ nm. This corresponds to the lowest carrier density of $n_{min} \approx \pm 2.2 \times 10^{12}$ cm^{-2} for the position of the SDPs (red dashed lines in Figure 2a). The orientation of the MSL is described by the angle θ relative to the graphene lattice

$$\tan\theta = \frac{-\sin\phi}{(1+\delta)-\cos\phi} \quad (2)$$

For the graphene/hBN system, one finds $|\theta| \lesssim 80°$.[29] These two equations describe the top 2L-MSL and the bottom 2L-MSL, as shown schematically in Figure 1. The functional dependence of λ and θ on ϕ is plotted in Supporting Information Figure S1.

In a fully encapsulated graphene device, not only one, but both hBN layers can be aligned to the graphene layer so that two graphene/hBN 2L-MSLs can form. In this case, the potential modulations of the two 2L-MSLs are superimposed and form a MSL with a third periodicity. The values of the resulting periods can be understood based on Figure 3a. The

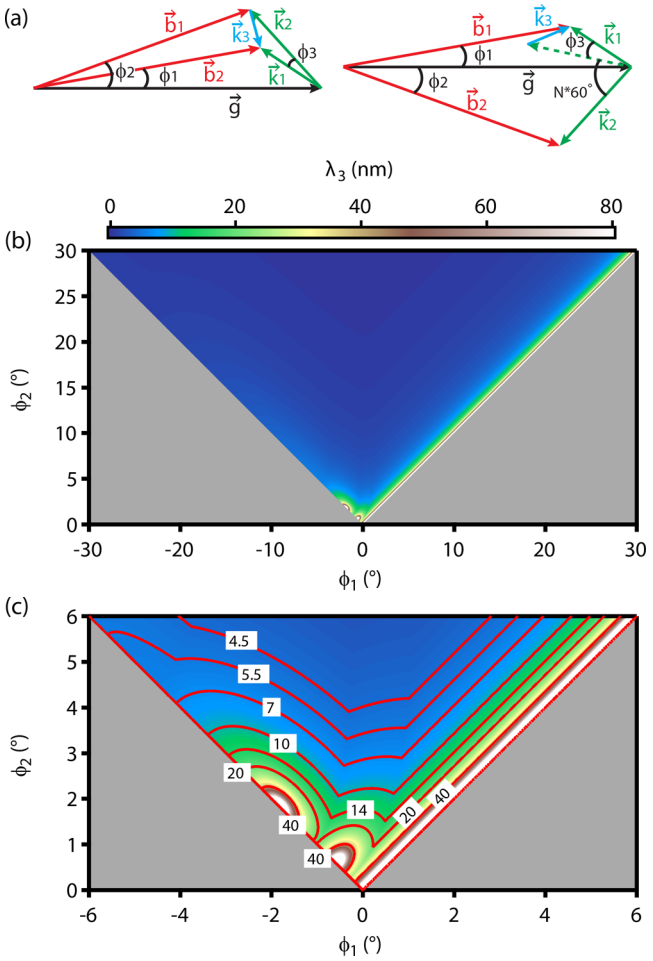

Figure 3. (a) Schematics in reciprocal space for the formation of different MSLs, where $\vec{g}$, $\vec{b}_1$, $\vec{b}_2$, $\vec{k}_1$, $\vec{k}_2$, and $\vec{k}_3$ are one of the reciprocal lattice vectors for graphene, top hBN, bottom hBN, top 2L-MSL, bottom 2L-MSL, and 3L-MSL, respectively. N is an integer, which can be 1, 2, or 3. (b) λ_3 plotted as a function of ϕ_1 and ϕ_2 for all possible twist angles. (c) Zoom-in of (b) for small twist angles. Numbers on the contour lines indicate the values of λ_3 in nm.

vectors $\vec{g}$, $\vec{b}_1$, and $\vec{b}_2$ denote one of the reciprocal lattice vectors for the graphene, the top hBN, and the bottom hBN layers, respectively. The twist angle between the top (bottom) hBN and graphene is denoted ϕ_1 (ϕ_2). Following the derivations in refs 29 and 33, one of the top 2L-MSL (bottom 2L-MSL) reciprocal lattice vectors $\vec{k}_1$ ($\vec{k}_2$) is given by the vector connecting $\vec{g}$ to $\vec{b}_1$ ($\vec{b}_2$). The moiré period $\lambda_{1,2}$ is then given by $\lambda_{1,2} = 4\pi/(\sqrt{3}|\vec{k}_{1,2}|)$, which is explicitly described by eq 1 as a function of the twist angle $\phi_{1,2}$. Since the reciprocal lattices of the top 2L-MSL and the bottom 2L-MSL are triangular, the same as those for graphene and hBN, we can use the same approach to derive the 3L-MSL, which is described by the

DOI: 10.1021/acs.nanolett.8b05061
Nano Lett. 2019, 19, 2371−2376

vector connecting $\vec{k}_2$ to $\vec{k}_1$, denoted $\vec{k}_3$. The 3L-MSL period is then given by $\lambda_3 = 4\pi/(\sqrt{3}|\vec{k}_3|)$.

In order to calculate λ_3 using eq 1, we first need to find the new a, δ, and ϕ. Because of symmetry, we only consider $\phi_1 < \phi_2$, so λ_2, the smaller period of the two graphene/hBN 2L-MSLs, becomes the new a and the new δ will then be given by $(\lambda_1 - \lambda_2)/\lambda_2$. The new ϕ, denoted ϕ_3, is determined by $|\theta_1 - \theta_2|$, where θ_1 (θ_2) is the relative orientation of the top 2L-MSL (bottom 2L-MSL) with respect to the graphene lattice, described by eq 2. Different cases occur for ϕ_3 due to the 60° rotational symmetry of the lattices. Since ϕ in eq 1 is defined for −30° to 30°, we subtract multiples of 60° to bring ϕ_3 to this range if it is larger than 30°, given as

$$\phi_3 = \begin{cases} |\theta_1 - \theta_2| & \text{if } 0 < |\theta_1 - \theta_2| \leqslant 30° \\ |\theta_1 - \theta_2| - 60° & \text{if } 30° < |\theta_1 - \theta_2| \leqslant 90° \\ |\theta_1 - \theta_2| - 120° & \text{if } 90° < |\theta_1 - \theta_2| \leqslant 150° \\ |\theta_1 - \theta_2| - 180° & \text{if } 150° < |\theta_1 - \theta_2| \leqslant 180°. \end{cases}$$

For the first case, the 3L-MSL is effectively the MSL formed by the two hBN layers, as illustrated in the left panel of Figure 3a. Another case is shown in the right panel, where multiples of 60° are subtracted, which is equivalent to choosing another reciprocal lattice vector for $\vec{k}_2$ so that it makes an angle within ±30° with $\vec{k}_1$.

Figure 3b plots all possible values for λ_3, as a function of ϕ_1 and ϕ_2, by using eq 1 with the new parameters. Theoretically λ_3 varies from below 1 nm to infinity, but one finds values larger than 14 nm only for small twist angles (see Figure 3c). For most angles λ_3 is very small, which explains why MSLs with periods larger than 14 nm have not been reported in previous studies, where only one hBN layer was aligned intentionally to the graphene layer.

Most of Figure 3c can be understood intuitively. On the line of the right diagonal with $\phi_1 \equiv \phi_2$, we have $\lambda_1 = \lambda_2$ and $\theta_1 = \theta_2$, therefore $\phi_3 = 0$, which results in $\lambda_3 = \infty$. This case is similar to the twisted bilayer graphene with a twist angle of 0, which does not form a MSL (or a MSL with infinitely large period). On the diagonal line in the left part with $\phi_1 \equiv -\phi_2$, one has $\lambda_1 = \lambda_2$, but $\theta_1 = -\theta_2$. As $|\phi_1| = |\phi_2|$ increases, $\theta_1 = -\theta_2$ evolves (see Supporting Information Figure S1). Therefore, ϕ_3 can have nonzero values, resulting in different λ_3 values. This case is again similar to the twisted bilayer graphene, but with a tunable twist angle. Whenever the difference of the orientation of the top 2L-MSL and the bottom 2L-MSL becomes multiples of 60° (i.e., $\theta_1 = -\theta_2 = 30°$ or 60°), the arrangement is equivalent to the full alignment of the two 2L-MSL due to the 60° rotational symmetry of the MSLs. In this case, ϕ_3 is reset to 0, therefore λ_3 diverges, giving rise to the two maxima, which is equivalent to the diagonal on the right part. The kinks on the contour lines come from the 60° rotational symmetry of the lattices, where $|\phi_3| = 30°$.

We now compare this simple model to our experiments. From the SDPs at $n_{S_A} \approx \pm 2.4 \times 10^{12}$ cm^{-2}, we calculate the corresponding moiré period $\lambda_1 \approx 13.2$ nm and the twist angle $|\phi_1| \approx 0.34$. Similarly, for the extrapolated SDP at $n_{S_B} \approx -5.2 \times 10^{12}$ cm^{-2}, we obtain $\lambda_2 \approx 9$ nm and $|\phi_2| \approx 1.2°$. The two twist angles give us two points in the map in Figure 3c: ∼17.2 nm for (0.34°, 1.2°) and ∼27.1 nm for (−0.34°, 1.2°). The ∼17.2 nm matches very well the value ∼17.3 nm extracted from the new-generation SDPs at $n_{S_C} \approx \pm 1.4 \times 10^{12}$ cm^{-2} in the transport measurement, which confirms that the new-generation SDPs come from the 3L-MSL.

We fabricated five hBN/graphene/hBN heterostructures in total, two of which exhibit 3L-MSL features. Data from devices of the second heterostructure are presented in the Supporting Information, which has a 3L-MSL with $\lambda_3 \approx 29.6$ nm.

In conclusion, we have demonstrated the emergence of a new generation of MSLs in fully encapsulated graphene devices with aligned top and bottom hBN layers. In these devices, we find three different superlattice periods, one of which is larger than the maximum graphene/hBN moiré period, which we attribute to the combined top and bottom hBN potential modulation. Whereas our model describes qualitatively the densities where these 3L-MSL features occur, the precise nature of the band structure distortions is unknown. The alignment of both hBN layers to graphene opens new possibilities for graphene band structure engineering, therefore providing motivation for further studies. Our new approach of MSL engineering is not limited to graphene with hBN but applies to two-dimensional materials in general, such as twisted trilayer graphene, graphene with transition metal dichalcogenides, and so forth, which might open a new direction in "twistronics".[55,56]

■ ASSOCIATED CONTENT

Supporting Information

The Supporting Information is available free of charge on the ACS Publications website at DOI: 10.1021/acs.nanolett.8b05061.

Discussions about fabrication, functional dependence of moiré period λ and orientation θ on the twist angle ϕ for 2L-MSL, data of other devices from the first hBN/graphene/hBN heterostructure and data of devices from the second heterostructure (PDF)

■ AUTHOR INFORMATION

Corresponding Authors

*E-mail: lujun.wang@unibas.ch.
*E-mail: andreas.baumgartner@unibas.ch.

ORCID

Lujun Wang: 0000-0002-5447-0484
Péter Makk: 0000-0001-7637-4672
Christian Schönenberger: 0000-0002-5652-460X

Notes

The authors declare no competing financial interest.

■ ACKNOWLEDGMENTS

This work has received funding from the Swiss Nanoscience Institute (SNI), the ERC project TopSupra (787414), the European Union Horizon 2020 research and innovation programme under Grant Agreement 696656 (Graphene Flagship), the Swiss National Science Foundation, the Swiss NCCR QSIT, Topograph, ISpinText FlagERA network and from the OTKA FK-123894 grants. P.M. acknowledges support from the Bolyai Fellowship, the Marie Curie grant and the National Research, Development and Innovation Fund of Hungary within the Quantum Technology National Excellence Program (Project Nr. 2017-1.2.1-NKP-2017-00001). M.-H.L. acknowledges financial support from Taiwan Minister of Science and Technology (MOST) under Grant

DOI: 10.1021/acs.nanolett.8b05061
Nano Lett. 2019, 19, 2371−2376

107-2112-M-006-004-MY3. Growth of hexagonal boron nitride crystals was supported by the Elemental Strategy Initiative conducted by the MEXT, Japan and the CREST (JPMJCR15F3), JST. The authors thank David Indolese and Peter Rickhaus for fruitful discussions.

REFERENCES

(1) Weiss, D.; Klitzing, K. V.; Ploog, K.; Weimann, G. Magneto-resistance Oscillations in a Two-Dimensional Electron Gas Induced by a Submicrometer Periodic Potential. *Europhys. Lett.* **1989**, *8*, 179.
(2) Weiss, D.; Roukes, M. L.; Menschig, A.; Grambow, P.; von Klitzing, K.; Weimann, G. Electron pinball and commensurate orbits in a periodic array of scatterers. *Phys. Rev. Lett.* **1991**, *66*, 2790−2793.
(3) Pfannkuche, D.; Gerhardts, R. R. Theory of magnetotransport in two-dimensional electron systems subjected to weak two-dimensional superlattice potentials. *Phys. Rev. B: Condens. Matter Mater. Phys.* **1992**, *46*, 12606−12626.
(4) Ferry, D. Quantum magnetotransport in lateral surface superlattices. *Prog. Quantum Electron.* **1992**, *16*, 251−317.
(5) Schlösser, T.; Ensslin, K.; Kotthaus, J. P.; Holland, M. Internal structure of a Landau band induced by a lateral superlattice: a glimpse of Hofstadter's butterfly. *Europhys. Lett.* **1996**, *33*, 683.
(6) Albrecht, C.; Smet, J. H.; Weiss, D.; von Klitzing, K.; Hennig, R.; Langenbuch, M.; Suhrke, M.; Rössler, U.; Umansky, V.; Schweizer, H. Fermiology of Two-Dimensional Lateral Superlattices. *Phys. Rev. Lett.* **1999**, *83*, 2234−2237.
(7) Albrecht, C.; Smet, J. H.; von Klitzing, K.; Weiss, D.; Umansky, V.; Schweizer, H. Evidence of Hofstadter's Fractal Energy Spectrum in the Quantized Hall Conductance. *Phys. Rev. Lett.* **2001**, *86*, 147−150.
(8) Geisler, M. C.; Smet, J. H.; Umansky, V.; von Klitzing, K.; Naundorf, B.; Ketzmerick, R.; Schweizer, H. Detection of a Landau Band-Coupling-Induced Rearrangement of the Hofstadter Butterfly. *Phys. Rev. Lett.* **2004**, *92*, 256801.
(9) Castro Neto, A. H.; Guinea, F.; Peres, N. M. R.; Novoselov, K. S.; Geim, A. K. The electronic properties of graphene. *Rev. Mod. Phys.* **2009**, *81*, 109−162.
(10) Park, C.-H.; Yang, L.; Son, Y.-W.; Cohen, M. L.; Louie, S. G. Anisotropic behaviours of massless Dirac fermions in graphene under periodic potentials. *Nat. Phys.* **2008**, *4*, 213.
(11) Park, C.-H.; Yang, L.; Son, Y.-W.; Cohen, M. L.; Louie, S. G. New Generation of Massless Dirac Fermions in Graphene under External Periodic Potentials. *Phys. Rev. Lett.* **2008**, *101*, 126804.
(12) Barbier, M.; Peeters, F. M.; Vasilopoulos, P.; Pereira, J. M. Dirac and Klein-Gordon particles in one-dimensional periodic potentials. *Phys. Rev. B: Condens. Matter Mater. Phys.* **2008**, *77*, 115446.
(13) Brey, L.; Fertig, H. A. Emerging Zero Modes for Graphene in a Periodic Potential. *Phys. Rev. Lett.* **2009**, *103*, No. 046809.
(14) Sun, J.; Fertig, H. A.; Brey, L. Effective Magnetic Fields in Graphene Superlattices. *Phys. Rev. Lett.* **2010**, *105*, 156801.
(15) Burset, P.; Yeyati, A. L.; Brey, L.; Fertig, H. A. Transport in superlattices on single-layer graphene. *Phys. Rev. B: Condens. Matter Mater. Phys.* **2011**, *83*, 195434.
(16) Ortix, C.; Yang, L.; van den Brink, J. Graphene on incommensurate substrates: Trigonal warping and emerging Dirac cone replicas with halved group velocity. *Phys. Rev. B: Condens. Matter Mater. Phys.* **2012**, *86*, No. 081405.
(17) Dubey, S.; Singh, V.; Bhat, A. K.; Parikh, P.; Grover, S.; Sensarma, R.; Tripathi, V.; Sengupta, K.; Deshmukh, M. M. Tunable Superlattice in Graphene To Control the Number of Dirac Points. *Nano Lett.* **2013**, *13*, 3990−3995.
(18) Drienovsky, M.; Schrettenbrunner, F.-X.; Sandner, A.; Weiss, D.; Eroms, J.; Liu, M.-H.; Tkatschenko, F.; Richter, K. Towards superlattices: Lateral bipolar multibarriers in graphene. *Phys. Rev. B: Condens. Matter Mater. Phys.* **2014**, *89*, 115421.
(19) Drienovsky, M.; Joachimsmeyer, J.; Sandner, A.; Liu, M.-H.; Taniguchi, T.; Watanabe, K.; Richter, K.; Weiss, D.; Eroms, J. Commensurability Oscillations in One-Dimensional Graphene Superlattices. *Phys. Rev. Lett.* **2018**, *121*, No. 026806.
(20) Sun, Z.; Pint, C. L.; Marcano, D. C.; Zhang, C.; Yao, J.; Ruan, G.; Yan, Z.; Zhu, Y.; Hauge, R. H.; Tour, J. M. Towards hybrid superlattices in graphene. *Nat. Commun.* **2011**, *2*, 559.
(21) Bai, J.; Zhong, X.; Jiang, S.; Huang, Y.; Duan, X. Graphene nanomesh. *Nat. Nanotechnol.* **2010**, *5*, 190.
(22) Sandner, A.; Preis, T.; Schell, C.; Giudici, P.; Watanabe, K.; Taniguchi, T.; Weiss, D.; Eroms, J. Ballistic Transport in Graphene Antidot Lattices. *Nano Lett.* **2015**, *15*, 8402−8406.
(23) Yagi, R.; Sakakibara, R.; Ebisuoka, R.; Onishi, J.; Watanabe, K.; Taniguchi, T.; Iye, Y. Ballistic transport in graphene antidot lattices. *Phys. Rev. B: Condens. Matter Mater. Phys.* **2015**, *92*, 195406.
(24) Zhang, Y.; Kim, Y.; Gilbert, M. J.; Mason, N. Electronic transport in a two-dimensional superlattice engineered via self-assembled nanostructures. *npj 2D Materials and Applications* **2018**, *2*, 31.
(25) Forsythe, C.; Zhou, X.; Watanabe, K.; Taniguchi, T.; Pasupathy, A.; Moon, P.; Koshino, M.; Kim, P.; Dean, C. R. Band structure engineering of 2D materials using patterned dielectric superlattices. *Nat. Nanotechnol.* **2018**, *13*, 566−571.
(26) Dean, C. R.; Young, A. F.; Meric, I.; Lee, C.; Wang, L.; Sorgenfrei, S.; Watanabe, K.; Taniguchi, T.; Kim, P.; Shepard, K. L.; Hone, J. Boron nitride substrates for high-quality graphene electronics. *Nat. Nanotechnol.* **2010**, *5*, 722.
(27) Decker, R.; Wang, Y.; Brar, V. W.; Regan, W.; Tsai, H.-Z.; Wu, Q.; Gannett, W.; Zettl, A.; Crommie, M. F. Local Electronic Properties of Graphene on a BN Substrate via Scanning Tunneling Microscopy. *Nano Lett.* **2011**, *11*, 2291−2295.
(28) Xue, J.; Sanchez-Yamagishi, J.; Bulmash, D.; Jacquod, P.; Deshpande, A.; Watanabe, K.; Taniguchi, T.; Jarillo-Herrero, P.; LeRoy, B. J. Scanning tunnelling microscopy and spectroscopy of ultra-flat graphene on hexagonal boron nitride. *Nat. Mater.* **2011**, *10*, 282.
(29) Yankowitz, M.; Xue, J.; Cormode, D.; Sanchez-Yamagishi, J. D.; Watanabe, K.; Taniguchi, T.; Jarillo-Herrero, P.; Jacquod, P.; LeRoy, B. J. Emergence of superlattice Dirac points in graphene on hexagonal boron nitride. *Nat. Phys.* **2012**, *8*, 382.
(30) Kindermann, M.; Uchoa, B.; Miller, D. L. Zero-energy modes and gate-tunable gap in graphene on hexagonal boron nitride. *Phys. Rev. B: Condens. Matter Mater. Phys.* **2012**, *86*, 115415.
(31) Wallbank, J. R.; Patel, A. A.; Mucha-Kruczyński, M.; Geim, A. K.; Fal'ko, V. I. Generic miniband structure of graphene on a hexagonal substrate. *Phys. Rev. B: Condens. Matter Mater. Phys.* **2013**, *87*, 245408.
(32) Song, J. C. W.; Shytov, A. V.; Levitov, L. S. Electron Interactions and Gap Opening in Graphene Superlattices. *Phys. Rev. Lett.* **2013**, *111*, 266801.
(33) Moon, P.; Koshino, M. Electronic properties of graphene/hexagonal-boron-nitride moiré superlattice. *Phys. Rev. B: Condens. Matter Mater. Phys.* **2014**, *90*, 155406.
(34) Ponomarenko, L. A.; Gorbachev, R. V.; Yu, G. L.; Elias, D. C.; Jalil, R.; Patel, A. A.; Mishchenko, A.; Mayorov, A. S.; Woods, C. R.; Wallbank, J. R.; Mucha-Kruczynski, M.; Piot, B. A.; Potemski, M.; Grigorieva, I. V.; Novoselov, K. S.; Guinea, F.; Fal'ko, V. I.; Geim, A. K. Cloning of Dirac fermions in graphene superlattices. *Nature* **2013**, *497*, 594.
(35) Dean, C. R.; Wang, L.; Maher, P.; Forsythe, C.; Ghahari, F.; Gao, Y.; Katoch, J.; Ishigami, M.; Moon, P.; Koshino, M.; Taniguchi, T.; Watanabe, K.; Shepard, K. L.; Hone, J.; Kim, P. Hofstadter's butterfly and the fractal quantum Hall effect in moiré superlattices. *Nature* **2013**, *497*, 598.
(36) Hunt, B.; Sanchez-Yamagishi, J. D.; Young, A. F.; Yankowitz, M.; LeRoy, B. J.; Watanabe, K.; Taniguchi, T.; Moon, P.; Koshino, M.; Jarillo-Herrero, P.; Ashoori, R. C. Massive Dirac Fermions and Hofstadter Butterfly in a van der Waals Heterostructure. *Science* **2013**, *340*, 1427−1430.
(37) Yu, G. L.; Gorbachev, R. V.; Tu, J. S.; Kretinin, A. V.; Cao, Y.; Jalil, R.; Withers, F.; Ponomarenko, L. A.; Piot, B. A.; Potemski, M.;

DOI: 10.1021/acs.nanolett.8b05061
Nano Lett. 2019, 19, 2371−2376

Elias, D. C.; Chen, X.; Watanabe, K.; Taniguchi, T.; Grigorieva, I. V.; Novoselov, K. S.; Fal'ko, V. I.; Geim, A. K.; Mishchenko, A. Hierarchy of Hofstadter states and replica quantum Hall ferromagnetism in graphene superlattices. *Nat. Phys.* **2014**, *10*, 525.
(38) Wang, L.; Gao, Y.; Wen, B.; Han, Z.; Taniguchi, T.; Watanabe, K.; Koshino, M.; Hone, J.; Dean, C. R. Evidence for a fractional fractal quantum Hall effect in graphene superlattices. *Science* **2015**, *350*, 1231−1234.
(39) Krishna Kumar, R.; Chen, X.; Auton, G. H.; Mishchenko, A.; Bandurin, D. A.; Morozov, S. V.; Cao, Y.; Khestanova, E.; Ben Shalom, M.; Kretinin, A. V.; Novoselov, K. S.; Eaves, L.; Grigorieva, I. V.; Ponomarenko, L. A.; Fal'ko, V. I.; Geim, A. K. High-temperature quantum oscillations caused by recurring Bloch states in graphene superlattices. *Science* **2017**, *357*, 181−184.
(40) Gorbachev, R. V.; Song, J. C. W.; Yu, G. L.; Kretinin, A. V.; Withers, F.; Cao, Y.; Mishchenko, A.; Grigorieva, I. V.; Novoselov, K. S.; Levitov, L. S.; Geim, A. K. Detecting topological currents in graphene superlattices. *Science* **2014**, *346*, 448−451.
(41) Woods, C. R.; Britnell, L.; Eckmann, A.; Ma, R. S.; Lu, J. C.; Guo, H. M.; Lin, X.; Yu, G. L.; Cao, Y.; Gorbachev, R.; Kretinin, A. V.; Park, J.; Ponomarenko, L. A.; Katsnelson, M. I.; Gornostyrev, Y.; Watanabe, K.; Taniguchi, T.; Casiraghi, C.; Gao, H.-J.; Geim, A. K.; Novoselov, K. Commensurate-incommensurate transition in graphene on hexagonal boron nitride. *Nat. Phys.* **2014**, *10*, 451.
(42) Shi, Z.; Jin, C.; Yang, W.; Ju, L.; Horng, J.; Lu, X.; Bechtel, H. A.; Martin, M. C.; Fu, D.; Wu, J.; Watanabe, K.; Taniguchi, T.; Zhang, Y.; Bai, X.; Wang, E.; Zhang, G.; Wang, F. Gate dependent pseudospin mixing in graphene/boron nitride moiré superlattices. *Nat. Phys.* **2014**, *10*, 743.
(43) Lee, M.; Wallbank, J. R.; Gallagher, P.; Watanabe, K.; Taniguchi, T.; Fal'ko, V. I.; Goldhaber-Gordon, D. Ballistic miniband conduction in a graphene superlattice. *Science* **2016**, *353*, 1526−1529.
(44) Wang, E.; Lu, X.; Ding, S.; Yao, W.; Yan, M.; Wan, G.; Deng, K.; Wang, S.; Chen, G.; Ma, L.; Jung, J.; Fedorov, A. V.; Zhang, Y.; Zhang, G.; Zhou, S. Gaps induced by inversion symmetry breaking and second-generation Dirac cones in graphene/hexagonal boron nitride. *Nat. Phys.* **2016**, *12*, 1111.
(45) Handschin, C.; Makk, P.; Rickhaus, P.; Liu, M.-H.; Watanabe, K.; Taniguchi, T.; Richter, K.; Schönenberger, C. Fabry-Pérot Resonances in a Graphene/hBN Moiré Superlattice. *Nano Lett.* **2017**, *17*, 328−333.
(46) Spanton, E. M.; Zibrov, A. A.; Zhou, H.; Taniguchi, T.; Watanabe, K.; Zaletel, M. P.; Young, A. F. Observation of fractional Chern insulators in a van der Waals heterostructure. *Science* **2018**, *360*, 62−66.
(47) Cao, Y.; Luo, J. Y.; Fatemi, V.; Fang, S.; Sanchez-Yamagishi, J. D.; Watanabe, K.; Taniguchi, T.; Kaxiras, E.; Jarillo-Herrero, P. Superlattice-Induced Insulating States and Valley-Protected Orbits in Twisted Bilayer Graphene. *Phys. Rev. Lett.* **2016**, *117*, 116804.
(48) Kim, K.; DaSilva, A.; Huang, S.; Fallahazad, B.; Larentis, S.; Taniguchi, T.; Watanabe, K.; LeRoy, B. J.; MacDonald, A. H.; Tutuc, E. Tunable moiré bands and strong correlations in small-twist-angle bilayer graphene. *Proc. Natl. Acad. Sci. U. S. A.* **2017**, *114*, 3364−3369.
(49) Rickhaus, P.; Wallbank, J.; Slizovskiy, S.; Pisoni, R.; Overweg, H.; Lee, Y.; Eich, M.; Liu, M.- H.; Watanabe, K.; Taniguchi, T.; Ihn, T.; Ensslin, K. Transport Through a Network of Topological Channels in Twisted Bilayer Graphene. *Nano Lett.* **2018**, *18*, 6725−6730.
(50) Cao, Y.; Fatemi, V.; Fang, S.; Watanabe, K.; Taniguchi, T.; Kaxiras, E.; Jarillo-Herrero, P. Unconventional superconductivity in magic-angle graphene superlattices. *Nature* **2018**, *556*, 43.
(51) Yankowitz, M.; Chen, S.; Polshyn, H.; Watanabe, K.; Taniguchi, T.; Graf, D.; Young, A. F.; Dean, C. R. Tuning superconductivity in twisted bilayer graphene. **2018**, arXiv:1808.07865.
(52) Cao, Y.; Fatemi, V.; Demir, A.; Fang, S.; Tomarken, S. L.; Luo, J. Y.; Sanchez-Yamagishi, J. D.; Watanabe, K.; Taniguchi, T.; Kaxiras, E.; Ashoori, R. C.; Jarillo-Herrero, P. Correlated insulator behaviour at half-filling in magic-angle graphene superlattices. *Nature* **2018**, *556*, 80.
(53) Wang, L.; Meric, I.; Huang, P. Y.; Gao, Q.; Gao, Y.; Tran, H.; Taniguchi, T.; Watanabe, K.; Campos, L. M.; Muller, D. A.; Guo, J.; Kim, P.; Hone, J.; Shepard, K. L.; Dean, C. R. One-Dimensional Electrical Contact to a Two-Dimensional Material. *Science* **2013**, *342*, 614−617.
(54) Chen, G.; Sui, M.; Wang, D.; Wang, S.; Jung, J.; Moon, P.; Adam, S.; Watanabe, K.; Taniguchi, T.; Zhou, S.; Koshino, M.; Zhang, G.; Zhang, Y. Emergence of Tertiary Dirac Points in Graphene Moiré Superlattices. *Nano Lett.* **2017**, *17*, 3576−3581.
(55) Carr, S.; Massatt, D.; Fang, S.; Cazeaux, P.; Luskin, M.; Kaxiras, E. Twistronics: Manipulating the electronic properties of two-dimensional layered structures through their twist angle. *Phys. Rev. B: Condens. Matter Mater. Phys.* **2017**, *95*, No. 075420.
(56) Ribeiro-Palau, R.; Zhang, C.; Watanabe, K.; Taniguchi, T.; Hone, J.; Dean, C. R. Twistable electronics with dynamically rotatable heterostructures. *Science* **2018**, *361*, 690−693.

NOTE ADDED AFTER ASAP PUBLICATION

This paper was published ASAP on March 7, 2019 with an error in the author affiliations. The revised paper was published on March 12, 2019.

DOI: 10.1021/acs.nanolett.8b05061
Nano Lett. 2019, 19, 2371−2376